Spatial and Temporal Variations of Blocking and Cyclogenesis in the 1978 / 79 Winter①

Hengyi Weng

Geophysical Fluid Dynamics Institute, Florida State University, Tallahassee, FL 32306, USA

Received March 21,1992

ABSTRACT

Complex empirical orthogonal function (CEOF) and Fourier analyses are applied to 500 hPa geopotential height anomaly for two selected latitude belts in the Northern Hemisphere from Dec 1978 through Feb 1979 based on the ECMWF FGGE III-b data. The positive anomalies in the three leading CEOFs for the high-latitude belt mainly show the preferred locations for blocking activity in the North Atlantic, the North Pacific and to the west of the Ural Mountains. The negative anomalies in the three leading CEOFs for the mid-latitude belt mainly show the preferred locations for cyclogenesis in the east coasts of Asia and North America, and the Mediterranean; weak cyclogenesis is also seen in the western United States and off the coasts of Spain and Morocco. The travelling components of the positive anomalies in the high-latitude belt mainly propagate westward, weakening as approaching the east side of some mountain chains while intensifying to the west side. On the contrary, the travelling components of the negative anomalies in the mid-latitude belt mainly propagate eastward, intensifying over the lee side of mountain and / or approaching the east coasts of the two continents. These preferred locations for blocking and cyclogenesis are basically consistent with the climatological results, and related to some teleconnection patterns found earlier.

The temporal variation of blocking highs seems to relate with the vacillation of the potential vorticity (PV) index defined by Weng (1992). There are two build-up stages of the PV index during the winter. Each build-up stage corresponds to a westward propagation of a large-scale positive anomaly in the high-latitude belt, resulting in the occurrence of a series of blocking highs over the western Eurasia, Scandinavia, Greenland and the Pacific. In general, the temporal variation of cyclogenesis is less reflected by the PV index than blocking highs. The duration of a PV index cycle of build-up and break-down is about 30-50 days. Within this low-frequency envelope, there is a global quasi-two-week vacillation of the PV index, reflecting one of the preferred time scales of mid-latitude cyclone and anticyclone activity in some preferred locations during the 1978 / 79 winter.

I. INTRODUCTION

Many climatological data analyses have revealed that although cyclones and anticyclones form in nearly every mid-latitude location, there is a strong tendency for cyclogenesis and blocking to occur in favored geographical locations.

Dole and Gordon (1983) analyzed the geographical persistence of 500 hPa geopotential height anomalies in the Northern Hemisphere for 14 winters, and found three major regions for the occurrence of persistent anomalies: the North Pacific to the south of the Aleutians (PAC), the North Atlantic to the southeast of Greenland (ATL), and the region from the northern Russia to the Arctic Ocean. Dole (1986) described the typical time-averaged structures of flow patterns occurring with persistent anomalies in these regions, and found that, for

①"Contribution No. 336" of Geophysical Fluid Dynamics Institute, FSU.

each region, the majority of persistent anomaly cases were associated with the amplification of a single, basic anomaly pattern, with one phase of the pattern being frequently associated with blocking. For the PAC and ATL regions, the primary patterns also resembled some teleconnection patterns discussed by Wallace and Gutzler (1981). By examining the daily 500 hPa geopotential height over the Northern Hemisphere for 15 years (1963–77), Shukla and Mo (1983) found that there were three distinct centers of maximum blocking activity: in the Pacific to the west of the Rockies, in the Atlantic to the west of the Alps and Scandinavian Mountain ranges, and to the west of the Ural Mountains. These preferred locations of persistent anomalies and their local structures do not change with season.

It is well know that cyclogenesis is concentrated in the lee of major mountain ranges and along the east coasts of Asia and North America, and that a major cyclogenetic region also exists in the Mediterranean in winter (e. g., Whittaker and Horn, 1984). Although cyclones may exist in relatively high latitudes, Gyakum et al. (1989) found that explosively intensified cyclones in North Pacific cold-season were almost exclusively south of 50°N, mainly between 30°–40°N. Moreover, based on the analyses for the period of 1958–77, Whittaker and Horn (1981) indicated that the greatest number of cyclogenesis in North America occurred between 35°N and 40°N. In their study of cyclogenesis over the East Asia during 1958–87, Chen et al. (1991) found that the cyclogenesis was much more active in the East China Sea between 30°N and 40°N than any other locations in the East Asia during wintertime.

The cyclogenesis along the east coasts of Asia and North America have been considered to be related to the Kuroshio current and the Gulf stream, respectively. Based on their climatological study of cyclogenesis over the East China Sea for the period of 1899–1962, Hanson and Long (1985) found that the area of maximum cyclogenesis in the Winter and early Spring was over the East China Sea to the southwest of Japan, overlying the Kuroshio current. Gyakum et al. (1989) analyzed eight-year (1975–83) cold-season surface cyclone activity,and indicated that most of the explosive cyclogenesis appears prominently in a region around Japan and the Kuroshio current. Bosart (1981) found a tongue of very warm SST parallel to the coast and 200km seaward in association with the Gulf stream during February 18–20, 1979, when a severe snow storm was reported at the east coast of the United States; the gradient of SST between nearshore and offshore at that time was about 2°C larger than a February climatological value.

The appearance and disappearance of active cyclones and anticyclones have also been seen to be related with zonal index cycles, which are defined in different ways by means of sea-level or aloft isobaric zonal winds, or zonal wind departure (Rossby et al., 1939; Namias, 1950; Kidson, 1985). In many cases, a "high" index is related with a strong midlatitude westerlies, while a "low" index is related with weak mid-latitude westerlies, often accompanied by cutoff cyclones and / or anticyclones.

Bell and Bosart (1989) completed a study about 15-year (1965–77) climatology of the Northern Hemisphere 500hPa closed cyclone and anticyclone centers. They noticed that mid-tropospheric closed cyclonic circulations are associated with a tropospheric region of anomalously high potential vorticity (PV), while closed anticyclonic circulations are associated with a stratospheric region of anomalously low PV. Their results are consistent with those found earlier by Hoskins et al. (1985).

Using the European Centre for Medium-range Weather Forecast (ECMWF) First GARP Global Experiment (FGGE) III-b data for the 1978 / 79 winter, Weng (1992) defined a PV index based on a zonally averaged, mid-latitude PV gradient on the 300K isentropic

surface. Weng found that the cross-correlation functions (c. c. f.) between the PV index and 500hPa geopotential height anomaly, at each grid point between 30°–80°N, brought out some teleconnection patterns revealed by climatological studies (e. g., Wallace and Gutzler, 1981). Each c.c.f. center reflected two geopotential height anomaly states observed in teleconnection patterns. For example, the negative c. c. f. center found over Scandinavia at lags 0 — +3 days suggested that Scandinavian highs tended to occur at or a few days after the minima of the PV index, while geopotential lows may be observed over there a few days after the maxima of the PV index. Therefore, blocking and cyclogenesis may be related to the PV index vacillation and teleconnection patterns.

The present study focuses on the spatial and temporal variations of blocking and cyclogenesis in the Northern Hemisphere during the FGGE winter by using complex EOF and Fourier analyses, and on the possible relationships between these variations and the PV index vacillation and the teleconnection patterns.

II. DATA SOURCE AND DEFINITIONS

The ECMWF FGGE level III-b data set for the winter period of December 1, 1978–February 28, 1979 twice daily (180 records) is used for the analyses. The data are at 3.75°× 1.875° latitude-longitude grid points for selected latitudes. All time series are diurnally detrended.

Two quantities related to the 500hPa geopotential height anomaly are defined as

$$\Phi_H = \frac{1}{4} \sum_{y=H} \varphi'(x,y,t) \tag{2.1}$$

and

$$\Phi_M = \frac{1}{3} \sum_{y=M} \varphi'(x,y,t), \tag{2.2}$$

where $\varphi'(x,y,t)$ is geopotential height anomaly from the zonal mean at longitude x, latitude y and time t; H and M refer to the high- and mid-latitude belts, respectively: H containing the data at 60°N, 63.75°N, 67.5°N and 71.25°N, while M containing those at 33.75°N, 37.50°N and 41.25°N. The intention to select such two latitude belts is to reduce a spatial degree of freedom, the latitude-dependence, while being able to capture some preferred locations for blocking and cyclogenesis. As seen from daily 500hPa maps (Bjørheim, 1981) as well as the climatological studies mentioned earlier, these latitude belts do include the major blocking and extratropical cyclogenesis regions.

As defined by Weng (1992), the PV index is a zonally averaged PV gradient between the two latitude belts on the 300K isentropic surface (averaged meridionally within each belt),

$$I = \frac{1}{4} \sum_{y=H} \overline{Q(x,y,t)}^x - \frac{1}{3} \sum_{y=M} \overline{Q(x,y,t)}^x, \tag{2.3}$$

where $Q(x,y,t)$ is the PV at longitude x, latitude y and time t; the overbar $-^x$ denotes a zonal average. As considered by Weng (1992), the choice of the 300K isentropic surface is partly because it intersects the 500hPa surface near 60°N in the US standard atmosphere in wintertime.

III. METHODOLOGY: COMPLEX EOF AND FOURIER ANALYSES

The complex EOF (empirical orthogonal function) analyses of Φ_H and Φ_M are performed following Pfeffer et al. (1990). Let ψ(x,t) be Φ_H or Φ_M ,

$$\psi(x,t)=\frac{1}{2}\sum_{p=1}^{N}[\psi_p(x,t)+\psi_p^*(x,t)]=\frac{1}{2}\sum_{n=1}^{N}[\Psi_n(t)e^{-inx}+\Psi_n^*(t)e^{-inx}], \tag{3.1}$$

where ψ_p is the p^{th} complex EOF component of ψ, Ψ_n is the n^{th} complex Fourier component of ψ, the asterisk stands for complex conjugate, N is the truncation level of the Fourier series used in the complex EOF analyses①. Ψ_n may be expanded as

$$\Psi_n(t)=\sum_{p=1}^{N}A_p(t)C_p(n), \tag{3.2}$$

where the function C_p(n) is constructed to be orthonormal, i. e., we demand that

$$\sum_{n=1}^{N}C_p(n)C_q^*(n)=\delta_{pq}, \tag{3.3}$$

where δ_{pq} is the Kronecker delta. The coefficient A_p(t) in (3.2), which represents the temporal structure of ψ_p, is calculated by projecting Ψ_n(t) onto C_p(n), i. e.,

$$A_p(t)=\sum_{n=1}^{N}\Psi_n(t)C_p^*(n). \tag{3.4}$$

The spatial structure of ψ_p is calculated as

$$B_p(x)=\sum_{n=1}^{N}e^{inx}C_p^*(n), \tag{3.5}$$

which represents the relative contribution from all the N Fourier modes to the pth complex EOF component. C_p(n) is the eigenvector with eigenvalue λ_p of the covariance matrix $C_{mn}=\overline{\Psi_n(t)\Psi_m^*(t)}$, given by the eigenvalue problem

$$\sum_{m=1}^{N}C_{mn}C_p(m)=\lambda_pC_p(n). \tag{3.6}$$

It can be shown that

$$\lambda_p=\overline{A_p(t)A_p^*(t)}, \tag{3.7}$$

where the overbar denotes a time average. Thus, the eigenvalue λ_p measures the variance residing in the p^{th} complex EOF component.

Let

$$\left.\begin{aligned}A_p(t)&=\alpha_p(t)e^{i\eta p(t)}\\B_p(t)&=\beta_p(t)e^{i\theta p(x)}\end{aligned}\right\}, \tag{3.8}$$

then, $\psi(x,t)$ can be expressed as

$$\psi(x,t)=\frac{1}{2}\sum_{p=1}^{N}[A_p(t)B_p^*(x)+A_p^*(t)B_p(x)], \tag{3.9}$$

①We have used 20 Fourier modes (N = 20) in the complex EOF analyses. Increasing N to 30 or more did not show appreciable changes in the results.

or

$$\psi(x,t) = \sum_{p=1}^{N} \alpha_p(t)\beta_p(x)\cos[\eta_p(t) - \theta_p(x)]. \tag{3.10}$$

The contours of ψ_p in a Hovmoller (longitude–time) diagram depict the spatial and temporal variations of ψ_p. The amplitude of ψ_p depends upon both functions $\alpha_p(t)$ and $\beta_p(x)$. The phase of ψ_p varies in longitude through $\theta_p(x)$, and in time through $\eta_p(t)$. The phase variation in longitude may be better seen through $\cos\theta_p(x)$ for a fixed time, and in time through $\cos\eta_p(t)$ for a fixed longitude, aside from a constant phase.

It can be shown that both $A_p(t)$ and $B_p(x)$ $(p=1,\cdots,N)$ are orthogonal. Since $C_p(n)$ is an eigenvector, it is natural to consider $B_p(x)$ as a base function, while $A_p(t)$ as a coefficient–the projection of ψ onto $B_p(x)$. Thus, we call $B_p(x)$ the p^{th} complex empirical orthogonal function (CEOF), while $A_p(t)$ the pth complex prinicpal component (CPC). It is easy to find that the amplitude of $B_p(x)$, $\beta_p(x)$, is dimensionless, and its magnitude is limited to $\sqrt{N}$, while $\alpha_p(t)$ is dimensional. The normalized amplitudes of $B_p(x)$ and $A_p(t)$ are $\beta'_p(x) = \beta_p(X) / \sqrt{N} < 1$ and $A'_p(x) = \sqrt{N} A_p(t)$, respectively.

The way to construct CEOFs and CPCs is not unique. The choice of the CEOFs in space and the CPCs in time in this work is based on the fact that we are interested in large–scale cyclones and anticyclones, defined in space rather than in time, so that we have transformed the data from grid points to the Fourier modes in space (in the wavenumber domain) before performing CEOF analyses. If we transformed the data from grid points to the Fourir modes in time (in the frequency domain) before performing CEOF analyses, we would get another set of CEOFs (in time, dimensionless) and CPCs (in space, dimensional). The transformation of data from grid points to Fourier modes is not necessary; however, it greatly simplifies the calculation in our analyses while keeping the essential information provided by the data. In the following discussion, for convenience, we will drop "complex" and use "EOF" instead of "CEOF"; specifically, we will use "EOFp" to mention the p^{th} complex EOF component of ψ, including its amplitudes and phases in both space and time.

Fourier analyses for each EOF are also performed as a complement.

IV. RESULTS

1. *High–latitude*, Φ_H 60°–71.25°N

(1). *EOF1*

Fig.1 shows EOF1 with 56.5% of the total variance. The pattern in the Hovmoller dia gram (Fig.1a) exhibits four intense positive anomaly centers which are quasi–stationary; three of them reach their maxima over Scandinavia while the remaining one is maximized over Greenland. These positive anomalies mainly reflect blocking episodes in Atlantic / European area. Thus, EOF1 may reflect one major area for blocking activity, i. e., in the Atlantic to the west of the Scandinavian Mountain ranges (Shukla and Mo, 1983). It is also consistent with the ATL persistent anomaly discussed by Dole and Gordon (1983).

There are strong negative anomaly centers extending from 60°E to150°E, a reflection of cyclogenetic activity in central Siberia, the lee of the Ural Mountains. There are also some weak negative anomalies over the Hudson Bay (75°–90°W), which coincides in time with the strong positive anomalies over the Atlantic / European area. These weak negative anomalies may reflect the quasi–stationary nature of the Hudson Bay low as discussed by Bell and

Bosart (1989). The concurrence of Greenland highs and Siberia lows, and that of Scandinavian highs and Hudson Bay lows, are indicative of the teleconnections analyzed by Weng (1992) for the FGGE winter.

Fig.1b shows the spatial amplitude of EOF1, which exhibits a broad maximum extending from Scandinavia to the Ural Mountains (10°–60°E), and a near-zero amplitude over the lee of the Mackenzie Mountains (120°W). Fig.1c suggests that within this spatial amplitude envelope, there is an asymmetric two-ridge wave. In Fig.1d, the temporal amplitude of EOF1 shows somewhat irregular oscillations, occurring on a long time scale of 3–4 weeks with shorter-period fluctuations. Fig.1e shows that the phase barely varies, except for one abrupt back-forth switch in each month, manifesting a quasi-stationary nature of EOF1.

Fourier analyses are performed in space and time for EOF1. Figs.2a, b show the spatial spectrum of $|\Phi_{H1}|^2$ (on a logarithmic scale) in the wavenumber domain for stationary and travelling waves, respectively. Most of the variance resides in the very low wavenumbers, the wavenumbers 1 and 2, in accord with Figs.1b, c. Moreover, the stationary wavenumber 1 is dominant, implying that this longest wave is quasi-stationary. Fig.2c shows the spectrum in the frequency domain. The dominant frequency is 4, corresponding to a period of 22.5-day, reflecting the four quite persistent episodes with positive anomaly over the Atlantic and negative anomaly over the Eurasia (Fig.1a). The second dominant frequency is 6, corresponding to a 15-day period, which reflects the existence of secondary maxima found between the primary maxima shown in Fig.1a.

(2). *EOF2*

Fig.3 shows EOF2 with 30.0% of the total variance. The pattern in Fig.3a, which shows large scale anomaly centers propagating westward, is completely different from that of EOF1 in Fig.1a. At a given time, there are often two positive and two negative anomaly centers around the world; one of the positive anomaly centers is much stronger than the other. The spatial structures of β_2 (Fig.3b) and $\cos\theta_2$ (Fig.3c) also have an asymmetric distribution in longitude; however, the amplitude structure is out-of-phase with that of EOF1: the wave amplifies over the northern Europe in EOF1, while over the Bering Sea and its vicinity in EOF2. Besides, the minimum of β_2 does not quite vanish. The temporal variation of α_2 (Fig.3d) indicates two build-up stages: from early December to early January, and from mid January to early February; the latter is weaker than the former. Fig.3e contains two quasi-stationary periods in mid December and mid-late February, and a quasi-periodic oscillation from late December to late January which is indicative of a travelling-wave character. Comparison of temporal amplitude variations between EOF1(Fig.1d) and EOF2(Fig.3d) shows that the sudden intensification of α_2 in early January may be related to the decay of α_1; nonlinear interaction between these two EOFs may be important during that time.

Unlike EOF1 where the main positive anomalies are over the Atlantic, the intense positive anomalies in EOF2 are over the north-eastern Pacific. These intense positive anomalies in EOF2 do correspond to blocking episodes in the Pacific, seen in daily 500hPa maps (Bjorheim et al., 1981). The block over the north-eastern Pacific and Alaska to the west of the Mackenzie Mountains (160°W) in early January may be originated in the northwestern Atlantic / Greenland in mid December, due to westward propagation of a large-scale positive anomaly. Similarly, following the positive anomaly originated over Siberia (110°E) around December 20, we find another westward propagation of a positive anomaly. This westward propagation may be responsible for spawning several positive anomaly centers

in that latitude belt at different times: the one to the west of the Ural Mountains (40°E) in early January, the one to the west of Baffin Island (80°W) in late January, and the one that reaches its maximum over the Bering Sea (180°W) at the beginning of February. EOF2 reflects the PAC persistent anomaly found by Dole and Gordon (1983) and some locations for blocking activity found by Shukla and Mo (1983).

The Fourier analyses shown in Figs.4a, b do convey the message of the presence of strong travelling waves in EOF2, with the wavenumber 2 component carrying the largest variance. In the frequency domain (Fig.4c), the dominant frequency is 1, corresponding to a 90-day period, which reflects the extreme development of the positive anomaly over the north-eastern Pacific and the negative anomaly over Greenland in early January; there is no competitive development in any other time during that winter. The less important frequencies 3 (30-day), 4(22.5-day) and 7(13-day) contain similar fraction of variance to each other.

(3). *EOF3*

Fig.5 shows EOF3 with 7.3% of the total variance. Although, compared to the first two EOFs, it contains a much smaller fraction of the total variance, its physical implication seems to be not too vague. It is a rather regular wave 3 pattern in space (Figs.5a, c), with the maximum amplitude near the Ural Mountains (60°E) and the minimum near 150°W (Fig.5b). The temporal variation of EOF3 (Figs.5d, e) shows much shorter time scales involved than those in EOF1 and EOF2.

When the traveling wave component is weak, the stationary component causes a main positive anomaly center around the Ural Mountains, with other two weaker positive anomaly centers over the Atlantic and the Pacific, respectively (Fig.5a). This is the case during the period from late January to mid February. During that period, the firsr two EOFs are relatively weak and α_1, α_2 and α_3 have comparable magnitudes, so that EOF3 plays a relatively important role. Another time period for EOF3 being relatively important is around December 17 when the main positive anomaly center is over Siberia (90°E). The westward propagation of this positive anomaly may also contribute to the Greenland high in late December.

The dominance of the wavenumber 3, especially of its travelling component, is also shown by Fourier analyses in the wavenumber domain (Figs. 6a, b). The Fourier analysis in the frequency domain (Fig.6c) shows a weak red-noise-like spectrum with a relatively large component of frequency 5 (18-day).

2. *Mid-latitude,* Φ_M (33.75°-41.25°N)

(1). *EOF1*

Fig.7 shows EOF1 with 31.6% of the total variance. The four-strip pattern in Fig.7a, as well as the four-wave spatial structure with its maximum amplitude in the western Pacific (Figs.7b, c), are basically consistent with the preferred geographical locations of cyclogenetic areas discussed by Bell and Bosart (1989), i. e., mainly along the east coasts of continents and in the lee of high mountain chains. The areas with negative anomaly revealed by EOF1 are: (i) the east coast of China / Pacific Ocean, in the lee of the Tibetan Plateau, extending from 90°E to 180°E with a maximum around 140°E; (ii) the east coast of the United States / Atlantic Ocean, in the lee of the Appalachians with a maximum around 65°W; (iii) the Mediterranean and Spain, in the lee of the Alps around 10°E; and (iv) the south-western United States. These negative anomalies are at their climatologically preferred locations.

Some negative anomaly centers travel eastward, within a limited longitude range, with a reoccurrence period of 1–2 weeks. Since β_1 has its primary maximum around 140°E and a secondary maximum around 70°W, with two minima around 60°E and 105°W, the cyclones in the areas of (i) and (ii) are much stronger than those in the areas of (iii) and (iv). Furthermore, the ones in (i) and (ii) have more travelling components than those in (iii) and (iv), reflecting the domains of the two major storm tracks within that latitude belt, where the influence of the Kuroshio Current and the Gulf Stream on the formation and development of cyclones is important. The East Asia–Pacific storm track is more intense compared with the one in the east coast of the United States, reflecting the fact that the North Pacific basin is the location with most developing cyclones in the Northern Hemisphere during the 1978 / 79 winter. This is consistent with Sanders and Gyakum (1980) who found that there were more "bombs" in the Pacific (west of 120°W) than in the Atlantic (east of 80°W) in December 78 and January 79, while the situation was opposite in February 79, which will be seen in EOF2 discussed below.

The Fourier analyses (Figs.8a, b) also show that the wavenumber 2 is dominant, with the stationary component having a larger variance than the travelling component. Thus, the spatial structure of EOF1 reflects major locations of cyclogenesis, especially in the east coast of China. The temporal variation exhibits more fluctuation in the amplitude (Fig.7d) and less switching in the phase (Fig.7e). The Fourier analysis in the frequency domain (Fig.8c) shows that the frequency 4 (22.5 days) is dominant, with the less dominant frequencies 8 (11 days) and 12 (5–6 days). Based on the ratios among the periods of 22.5 days, 11 days and 5–6 days, one is tempted to speculate that a period doubling mechanism in generating these time scales of cyclogenetic activity may be at work.

(2). *EOF2*

Fig.9 shows EOF2 with 20.3% of the total variance. This EOF mainly reflects an anomalous flow pattern over the east coast of the United States in the 1978 / 79 winter. Bosart (1981) reported that there were two anomalous warm periods and one cold period in the east coastal region of the United States in January and February. These are reflected in EOF2 by two periods with intensely positive geopotential height anomaly and one period with intensely negative anomaly near 80°W in these two months (Fig.9a). During the cold period, there were four snowstorms on January 31, and on February 7, 14 and 19. The centers of intense negative anomalies in EOF2 largely match the four snowstorms in time. β_2 has its maximum off the east coast of the United States, and a secondary maximum off the east coast of China (120°E) (Fig.9b). This spatial structure of β_2 is out-of-phase from that of β_1 (Fig.7b).

EOF2 may reflect an anomalous influence of the Gulf Stream on cyclogenesis off the east coast of the United States as revealed by Bosart (1981).

The dominant wavenumber, based on Fourier analyses, is the wavenumber 1 in both stationary and travelling components as seen in Figs.10a, b. This is consistent with Fig.9b where a remarkable amplitude peak is observed off the east coast of the United States. The dominant frequency in Fig.10c is 2, corresponding to a 45-day period, which appears to coincide with two persistent episodes observed during the 90-day winter.

(3). *EOF3*

Fig.11 shows EOF3 with 14.2% of the total variance. This EOF contains five distinct positive–negative anomaly regions around the latitude belt M (Figs.11a, c), with the largest

amplitude around 110°W (the Rocky Mountains) and 20°W (off the west coasts of Spain and Morocco) (Fig.11b). In Fig.11d, e, there is an aperiodic oscillation in the amplitude with small excursions; relatively large amplitudes are observed in early and mid December as well as in mid February. Also seen are abrupt phase switches in early and late January (Figs.11a, e).

If we focus on the area where β_3 looks like a "camel hump" (0°–160°W), i. e., over the area of Pacific–the western United States–the eastern United States–the Mediterranean, we find a positive–negative–positive–negative anomaly pattern, or its opposite state with negative–positive–negative–positive anomaly pattern for most days in December and February. These two patterns, with opposite anomalies over each location,are consistent with some teleconnection patterns discussed by Weng (1992). These anomaly patterns may result from the influence of two major teleconnection patterns: the Pacific / North America pattern (the first three locations), and a part of the North Atlantic Oscillation (the last two locations).

The Fourier analyses show the dominant wavenumbers 5 and 6 having both stationary and travelling components (Figs.12a, b), with the travelling components carrying more of the variance. In the frequency domain (Fig.11c) there are dominant frequencies 3 and 5, corresponding to 18– and 30–day periods, respectively.

V. DISCUSSIONS

Figs.13a, b give the sum of the first three EOFs of Φ_H and Φ_M, representing 93.8% and 66.1% of the total variance of Φ_H and Φ_M, respectively. The patterns in these figures are similar to those shown in Figs.14a, b which are based on the original grid–point data for the two latitude belts. Thus, the sums of the first three EOFs of Φ_H and Φ_M are good representatives of the original Φ_H and Φ_M, especially the one for Φ_H, in the 1978 / 79 winter.

We now follow the evolution of some anomaly centers in Figs.13 and 14, and relate it to the PV index vacillation shown in Fig.15. Starting in early December, a positive anomaly center emanating from Scandinavia propagates westward as shown in Figs.13a and 14a, when the PV index is in a "low" period as shown in Fig.15. There is a jog in the pass of the positive anomaly center in the Hovmoller diagrams. This jog results in a Greenland high and a Scandinavian high, corresponding to a secondary PV index maximum and a secondary PV index minimum in mid December. The jogged positive anomaly center then merges with another westward propagating positive anomaly center that has started off in Eurasian region in mid December. They coalesce into the intense Greenland high that attains to its maximum around December 21–22. The Greenland high coincides in time with two negative anomaly centers: one to the west (75°W) and the other to the east (10°W), shown in Fig.14b for Φ_M. When the Greenland high is getting mature, the two lows are merging into a single low, implying a dipole–blocking situation over the North Atlantic. A few days after the peak of the Greenland high, the PV index attains to another maximum. The large scale positive anomaly center of Φ_H continues propagating westward while weakening over Canada in late December. Meanwhile, the PV index is decreasing until the end of December when the PV index attains to a weak minimum. The westward propagating positive anomaly center re–amplifies after travelling over the Mackenzie Mountains in Alaska, where it contributes to the Pacific high which reaches its maximum around January 6. A few days after the peak of the Pacific high, the PV index attains to its primary maximum. It is seen in Fig.15 that during

the course when the PV index is building up from its primary minimum (early December) to its primary maximum (around January 9), the PV index has experienced several cycles with ascending secondary maxima and minima. This build-up time is about 40 days; it might be longer if the lowest PV value occurred prior to December 1, 1978.

When the PV index quickly decreases after January 9, the positive Φ_H center discussed earlier continues travelling westward with decreased intensity over the eastern Siberia. While travelling over the Ural Mountains, the positive anomaly re-amplifies and reaches the maximum over Scandinavia and the Norwegian Sea on January 18. Meanwhile, the PV index experiences its second build-up stage, which is basically similar to the first one. Corresponding to the PV index vacillation within the second build-up stage, the intensity of the large-scale positive anomaly center of Φ_H undergoes up-and-down variation while continuously propagating westward, resulting in the intense Greenland high around January 23 and the Pacific high around February 5. This course was discussed by Weng (1992). The synoptic and dynamic features of the above mentioned Eurasian high, the Scandinavian high and the Greenland high during the second half of January of 1979 have also been described by several authors (e. g., Bengtsson, 1981; Frederiksen and Bell, 1990; etc.). However, some studies viewed the occurrence in succession of these highs in a somewhat different way from that presented here. For example, Frederiksen and Bell (1990) concluded that the blocks over the North Atlantic were resulting from large-scale eastward propagating onset-of-blocking wave-train modes: after January 16, the North Atlantic block moved northeast to a location between Iceland and Scandinavia and coalesced with the western Eurasian block on January 18. However, the present study shows that the formation of the block over the region between Iceland and Scandinavia (a Scandinavian high) is mainly due to the westward propagation of the positive anomaly from the western Eurasia to Scandinavia, although a weak positive anomaly moving eastward from the North Atlantic is seen. The further westward propagation of that positive anomaly may also be responsible for the sudden weakening of the Scandinavian high and the intensifying of the Greenland high. During the course of the westward propagation, the intensity of the positive anomaly varies with location. This feature is seen from the behavior of the EOF1 of Φ_H. The Greenland high, appeared during January 22-25, coincides in time with several lows developing off the east coast of the United States and moving towards the East Atlantic, Spain / Mediterranean, as shown in Figs. 13b and 14b. This coincidence is consistent with the NAO teleconnection pattern discussed by Weng (1992), i. e., the 500hPa geopotential height anomaly over the southern Greenland and that over the east coast of the United States are negatively correlated through the PV index in that winter, which may result in a blocking situation over the North Atlantic. The westward propagation of the positive anomaly which results in Pacific highs during both build-up stages is mainly grasped by the EOF2 of Φ_H. It is anticipated that similar westward propagation of large-scale positive anomalies may have contributed to the fact that Pacific highs occurred after Atlantic highs for most of the 112 cases in 15 winters studied by Rex (1950).

In general, the travelling components of positive anomalies in the high-latitude belt mainly propagate westward, weakening as approaching the east side of some mountain chains while intensifying to the west side. On the contrary, the travelling components of negative anomalies in the mid-latitude belt mainly propagate eastward, intensifying over the lee side of mountains and / or approaching the east coasts of Asia and North America.

Since the first build-up stage of the PV index lasts about 40 days or longer, with a following break-down stage of about 6 days, and the second build-up stage lasts about 20 days, with a following break-down stage of about 13 days, the duration of a PV index cycle of build-up and break-down is about 30-50 days for the 1978 / 79 winter. It is not sure if there exists another build-up stage of the PV index after mid February. It is seen that during the three-month period, the PV index exhibits three primary minima corresponding to Scandinavian highs, and two primary maxima corresponding to Pacific highs. These highs exhibit blocking features. Some weaker Scandinavian highs are often observed around the times when the PV index experiences secondary minima. The Pacific highs are basically observed before the end of a PV index build-up stage, while Greenland highs are corresponding to some secondary maxima. As shown in Weng (1992), Scandinavia and its vicinity may be a key area of the global atmospheric circulation in that winter. The reoccurrence period of intense Scandinavian highs, which is about 30-50 days in the 1978 / 79 winter as shown in Figs. 13-15, is indicative of mid-tropospheric global circulation having such a low-frequency oscillation. Within this low-frequency envelope, there is a global quasi-two-week variation of the PV index, reflecting one of the preferred time scales of mid-latitude cyclone and anticyclone activity in some preferred locations during the 1978 / 79 winter.

Although the space in our EOF analyses is one dimensional, the two selected latitude belts seem to be able to grasp some preferred locations of active cyclones and anticyclones in the 1978 / 79 winter. The temporal variation of blocking highs seems to closely relate with the vacillation of the PV index. In general, the temporal variation of cyclogenesis is less reflected by the PV index than blocking highs. Because the zonally-averaged PV is much higher for the high-latitude belt than that for the mid-latitude belt, the variation of the mid-latitude PV related to cyclone activity is less influential to the PV index defined by Weng (1992). Thus, a weighted PV index may be needed to fairly relate with both blocking and cyclogenesis in different latitudes.

The data used here are limited to a single winter; all the discussions and conjectures given here should be viewed with caution. However, as a case study, the spatial and temporal variations of blocking and cyclogenesis in this winter revealed by the first three EOFs of Φ_H and Φ_M, and their relations to the PV index vacillation and teleconnection patterns discussed by Weng (1992), do reflect some important features found by previous authors based on climatological data.

I am deeply grateful to Dr. A. Barcilon and Dr. R. L. Pfeffer for their helpful discussions on this subject. Special thanks go to Prof. Baozhen Zhu for his stimulating comments during his visit at GFDI, FSU. Thanks also go to Y.-H. Chang, K. Convery, W. Auld and K.-D. Chen for their help in programming and plotting. This research was sponsored by NASA grant NAG 8-760 and NSF grant ATM-8802567. The computations were supported by the Florida State University through use of its supercomputer.

REFERENCES

Bell, G. D. and L. F. Bosart (1989), A 15-year climatology of Northern Hemisphere 500hPa closed cyclone and anticyclone centers, *Mon. Wea. Rev.*, **117**: 2142-2163.

Bengtsson, L. (1981), Numerical prediction of atmospheric blocking—A case study, *Tellus*, **33**:19-42.

Bjørheim, K., P. Julian, M. Kanamitsu, P. Kallberg, P. Price, S. Tracton, and S. Uppala (1981), FGGEIII-b daily global analyses, Part 1: December 1978-February 1979, *The European Centre for Medium Range Weather Forecasts*.

Bosart, L. F. (1981), The Presidents' Day snowstorm of 18-19 February 1979: A subsynoptic-scale event, *Mon. Wea.*

Rev., **109:** 1542–1566.

Chen, S. –J., Y. –H. Kuo, P. –Z. Zhang and Q. –F. Bai (1991), Synoptic climatology of cyclogenesis over East Asia, 1958–1987, *Mon. Wea. Rev.*, **119:**1407–1418.

Dole, R. M. (1986), Persistent anomalies of the extratropical Northern Hemisphere wintertime circulation: structure, *Mon. Wea. Rev.*, **114:** 178–207.

Dole, R. M. and N. D. Gordon (1983), Persistent anomalies of the extratropical Northern Hemisphere wintertime circulation: geographical distribution and regional persistence characteristics, *Mon. Wea. Rev.*, **111:** 1567–1586.

Frederiksen, J. S. and R. C. Bell (1990), North Atlantic blocking during January 1979: Linear theory, *Quart. J. Roy. Meteor. Soc.*, **116:** 1289–1313.

Gyakum, J. R., J. R. Anderson, R. H. Grumm and E. L. Gruner (1989), North Pacific coldseason surface cyclone activity: 1975–1983, *Mon. Wea. Rev.*, **117:** 1141–1155.

Hanson, H. P. and B.–S. Long (1985), Climatology of cyclogenesis over the East China Sea, *Mon. Wea. Rev.*, **113:** 697–707.

Hoskins, B. J., M. E. McIntyre, and A. W. Robertson (1985), On the use and significance of isentropic potential vorticity maps, *Quart. J. Roy. Meteor. Soc.*, **111:** 877–946.

Kidson, J. W. (1985), Index cycles in the Northern Hemisphere during the Global Weather Experiment, *Mon. Wea. Rev.*, **113:** 607–623.

Namias, J. (1950), *Extended range forecasting by mean circulation methods.*, U. S. Weather Bureau, Washington, DC, 55pp.

Pfeffer, R. L., J. Ahlquist, R. Kung, Y. Chang and G. Li (1990), A study of baroclinic wave behavior over bottom topography using complex principal component analysis of experimental data, *J. Atmos. Sci.*, **47:** 67–81.

Rex, D. F. (1950), Blocking action in the middle troposphere and its effect upon regional climate, II. The climatology of blocking action, *Tellus*, **2:** 275–301.

Rossby, C. –G., and Collaborators (1939), Relation between variations in the intensity of the zonal circulation of the atmosphere and the displacements of the semi–permanent centers of action, *J. Mar. Res.*, **2:** 38–55.

Sanders, F. and J. R. Gyakum (1980), Synoptic–dynamic climatology of the " bomb" , *Mon. Wea. Rev.*, **108:** 1589–1606.

Shukla, J. and K. C. Mo (1983), Seasonal and geographical variation of blocking, *Mon. Wea. Rev.*, **111:** 388–402.

Wallace, J. M. and D. S. Gutzler (1981),Teleconnections in the geopotential height field during the Northern Hemisphere winter, *Mon. Wea. Rev.*, **109:** 784–812.

Weng, H. –Y. (1992), Porential vorticity index vacillation in the 78–79 winter: its relation to telecommection patterns, *Quart. J. Roy. Meteor. Soc.*, in press.

Whirraker, L. M. and L. H. Horn (1981), Geographical and seaeonal distribution of North American cyclogenesis, 1958–1977, *Mon. Wea. Rev.*, **109:** 2312–2322.

Whittaker, L. M. and L. H. Horn (1984), Northern Hemisphere extratropical cyclone activity for four mid–season months, *J. climatol.* **4:** 297–310.

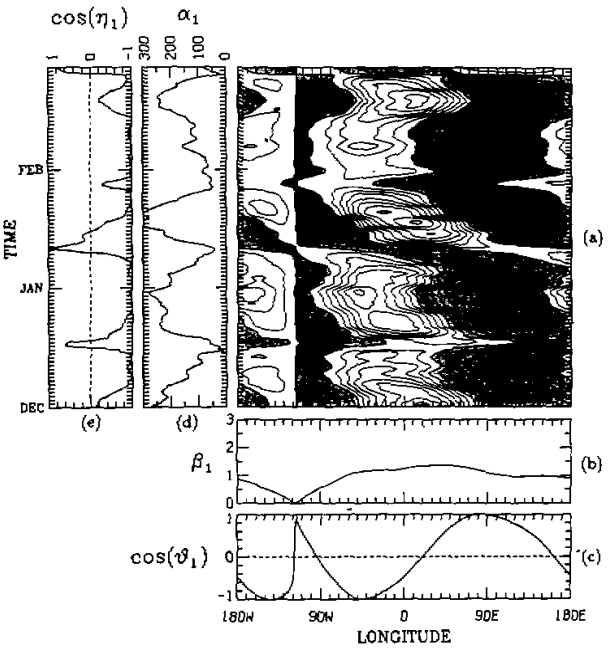

Fig.1. EOF1 for Φ_H (60°–71.25°N) for 180°W–180°E during Dec. 1978–Feb 1979: (a) the Hovmoller diagram, (b) the spatial amplitude,(c) the spatial phase, (d) the temporal amplitude, and (e) the temporal phase. Negative Φ_H anomalies in (a) are shaded. The contour interval in (a) is 50 m^2/s^2 (the unit geopotential meter). The unit in (d) is m^2/s^2.

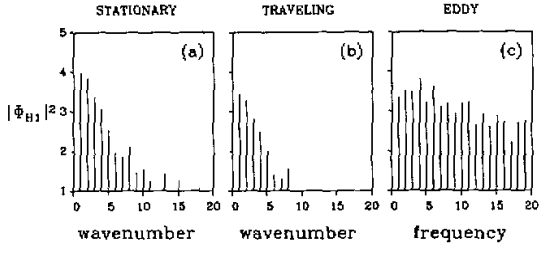

Fig.2. Fourier spectra of the variance contained in EOF1 of Φ_H for (a) stationary waves, (b) travelling waves, and (c) frequencies. The unit of the frequency is $1/90$ day^{-1}. $|\Phi_{H1}|^2$ (m^4/s^4) is plotted on a logarithmic scale.

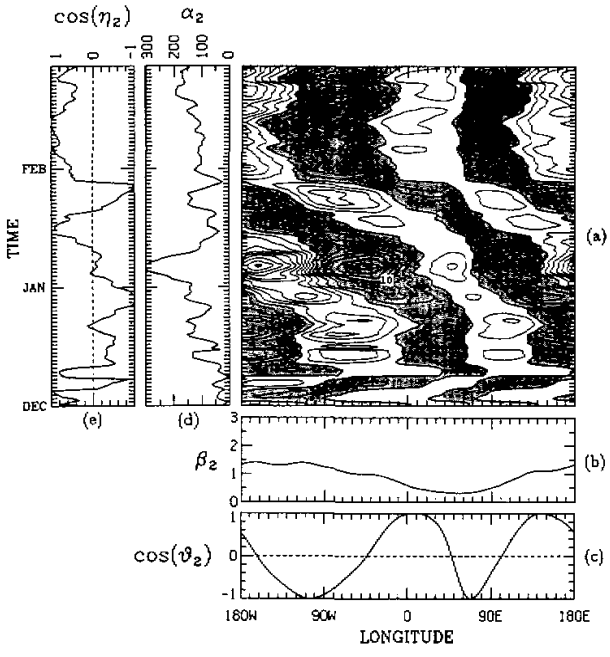

Fig.3. As in Fig. 1 except for EOF2 of Φ_H.

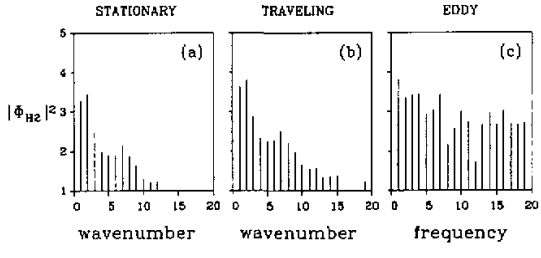

Fig.4. As in Fig. 2 except for EOF2 of Φ_H.

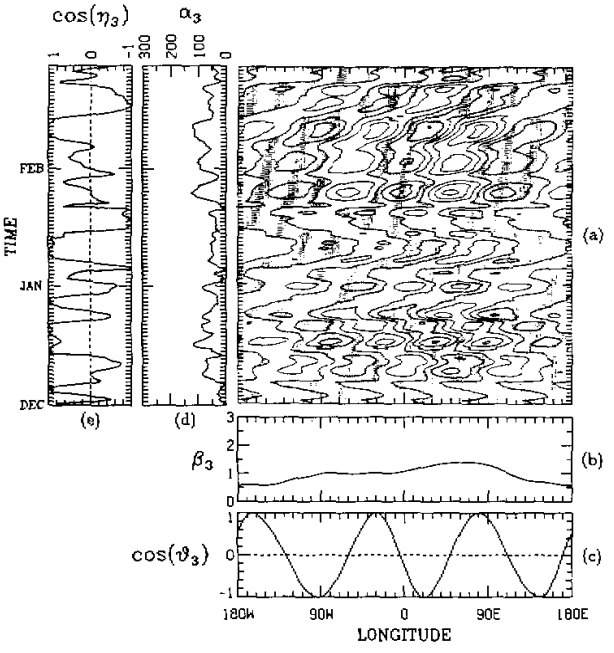

Fig.5. As in Fig. 1 except for EOF3 of Φ_H.

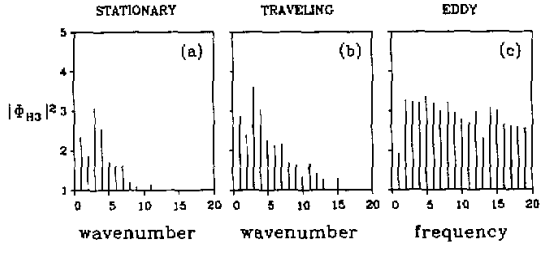

Fig.6. As in Fig. 2 except for EOF3 of Φ_H.

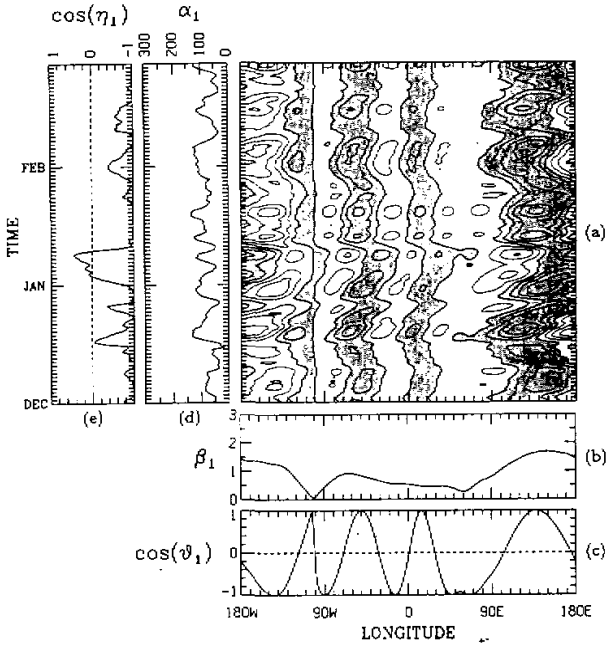

Fig.7. EOF1 for Φ_M (33.75°–41.25°N) for 180°W–180°E during Dec 1978–Feb 1979: (a) the Hovmoller diagram, (b) the spatial amplitude, (c) the spatial phase, (d) the temporal amplitude, and (e) the temporal phase. Negative Φ_H anomalies in (a) are shaded. The contour interval in (a) is 50 m^2 / s^2. The unit in (d) is m^2 / s^2.

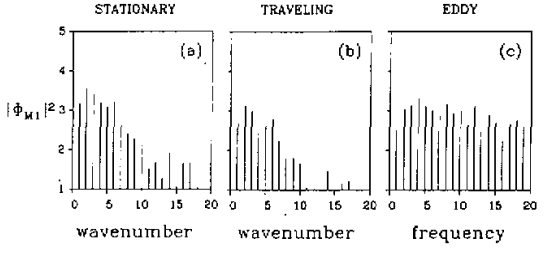

Fig.8. Fourier spectra of the variance contained in EOF1 of Φ_M for (a) stationary waves, (b) travelling waves, and (c) frequencies. The unit of the frequency is 1 / 90 day^{-1}. $|\Phi_{M1}|^2$ (m^4 / s^4) is plotted on a logarithmic scale.

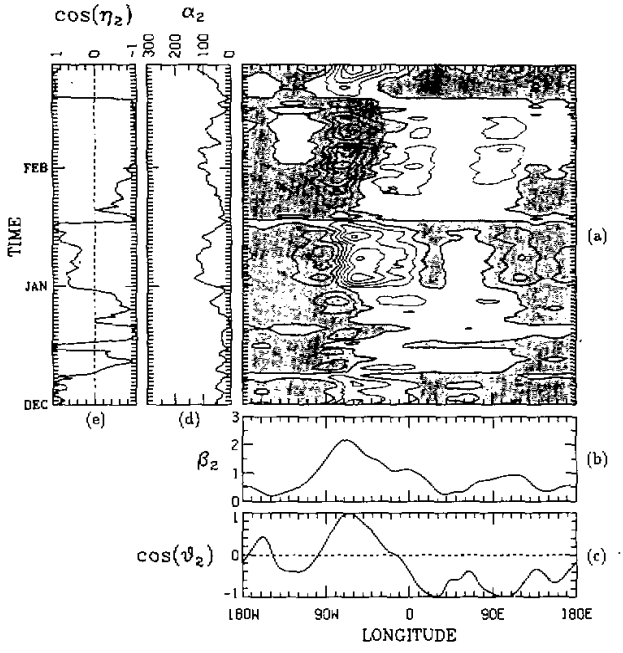

Fig.9. As in Fig. 7 except for EOF2 of Φ_M.

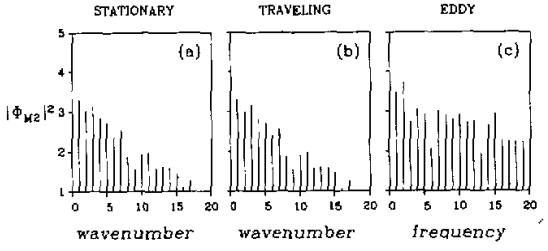

Fig.10. As in Fig. 8 except for EOF2 of Φ_M.

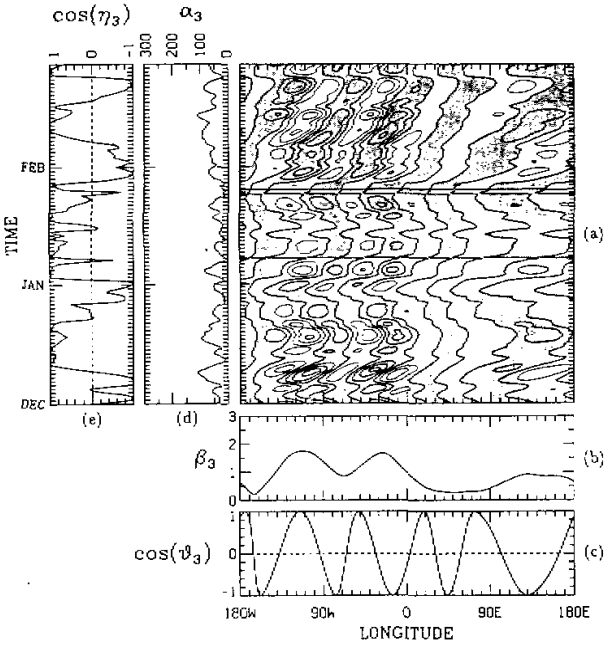

Fig.11. As in Fig. 7 except for EOF3 of Φ_M.

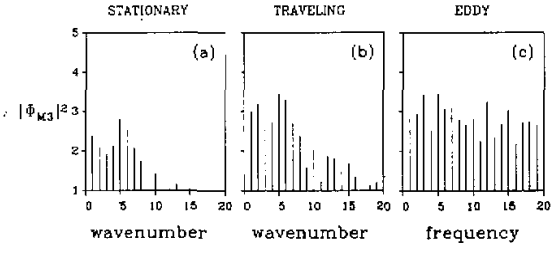

Fig.12. As in Fig. 8 except for EOF3 of Φ_M.

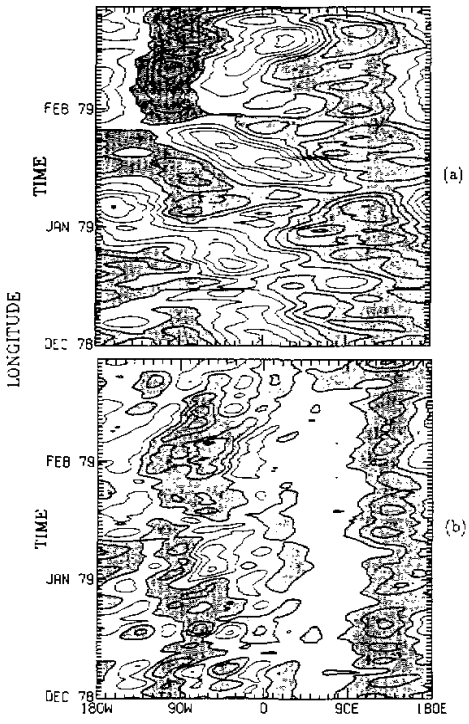

Fig.13. The Hovmoller diagrams for the sum of the three leading EOFs of (a) Φ_H and (b) Φ_M . The negative anomalies are shaded. The contour interval is 100 m^2/s^2.

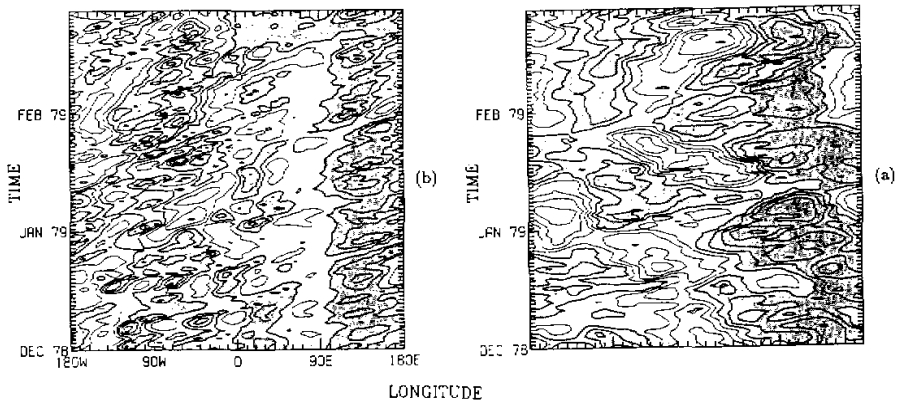

Fig.14. The Hovmoller diagrams for (a) Φ_H and Φ_M. The negative anomalies are shaded. The contour interval is $100m^2/s^2$.

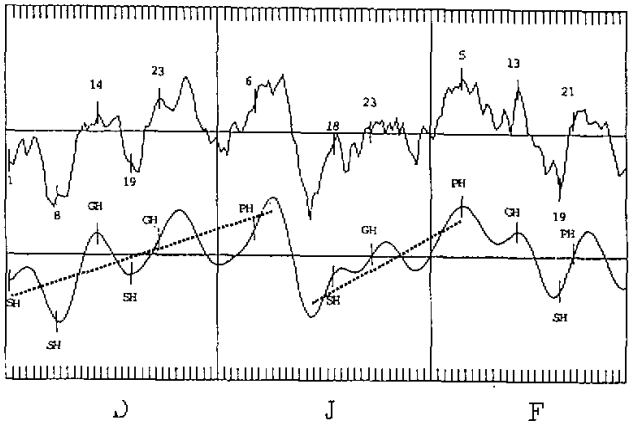

Fig.15. The PV (potential vorticity) index during December 1978–February 1979. The vertical apacing is equivalent to four standard deviations. The lower curve is a 7-day low-pass filtered time series. The dates with the extreme intensity of (SHs) Scandinavian highs, (GHs) Greenland highs and (PHs) Pacific highs are indicated. The two thick dash lines mark two PV index build-up stages (frome Weng, 1992).